Journal of Applied Geophysics 72 (2010) 129–140

Contents lists available at ScienceDirect

Journal of Applied Geophysics

journal homepage: www.elsevier.com/locate/jappgeo

Insights on surface wave dispersion and HVSR: Joint analysis via Pareto optimality

Dal Moro Giancarlo

GUtech (German University of Technology-affiliated RTWH, Aachen, Germany), PO Box 1816, Athaibah PC 130, Muscat, Oman

ARTICLE INFO

Article history:
Received 20 May 2010
Accepted 26 August 2010

Keywords:
Joint inversion
Surface wave dispersion
HVSR
Shear-wave velocity
Multi-Objective Evolutionary Algorithms
Rayleigh waves

ABSTRACT

Surface Wave (SW) dispersion and Horizontal-to-Vertical Spectral Ratio (HVSR) are known as tools able to provide possibly complementary information useful to depict the vertical shear-wave velocity profile. Their joint analysis might then be able to overcome the limits which inevitably affect such methodologies when they are singularly considered.

When a problem involves the optimization (i.e. the inversion) of two or more objectives, the standard practice is represented by a normalized summation able to account for the typically different nature and magnitude of the considered phenomena (thus objective functions). This way, a single cost function is obtained and the optimization problem is performed through standard solvers.

This approach is often problematic not only because of the mathematically and physically inelegant summation of quantities with different magnitudes and units of measurements. The critical point is indeed represented by the inaccurate performances necessarily obtained while dealing with problems characterized by several local minima and the impossibility of a rigorous assessment of the goodness and meaning of the final result.

In the present paper joint analysis of both synthetic and field SW dispersion curves and HVSR datasets is performed via the Pareto front analysis. Results show the relevance of Pareto's criterion not only as ranking system to proceed in heuristic optimization (Evolutionary Algorithms) but also as a tool able to provide some insights about the characteristics of the analyzed signals and the overall congruency of data interpretation and inversion.

Possible asymmetry of the final Pareto front models is discussed in the light of relative non-uniqueness of the two considered objective functions.

1. Introduction

Site characterization requires the determination of geomechanical properties often accomplished via non-invasive geophysical investigations. The employ of a single methodology necessarily brings some degree of uncertainty due both to possible ambiguity in data interpretation and non-uniqueness of the solution (e.g. Scales et al., 2001; Ivanov et al., 2005a,b; Dal Moro, 2008, 2010a; Palmer, 2010). Consequently, acquisition and joint analysis of further datasets is always highly recommended.

Surface Wave (SW) analysis is nowadays a popular method not only, as in past, for crustal studies (e.g. Evison et al., 1959) but for near-surface investigations as well (Glangeaud et al., 1999; Park et al., 1999; Dal Moro et al., 2007). The acronym *MASW* (*Multichannel Analysis of Surface Waves*), although could in principle indicate any kind of geophone-array-based study, is normally used for the active case while *ReMi* (*Refraction Microtremors*) commonly refers to linear-array passive experiments (e.g. Louie, 2001).

Though SW analysis potentially represents a fast and effective way to reconstruct the vertical V_S profile, problems connected with non-uniqueness of the solution (Luke et al., 2003), misinterpretation of data due both to mode misidentification (Zhang and Chan, 2003; Dal Moro, 2010a,b) and influence of guided waves (O'Neill et al., 2004; O'Neill and Matsuoka, 2005) pose some often poorly considered problems in SW analysis.

In order to put in evidence possible problems in SW dispersion curve interpretation, some synthetic seismograms were computed (Carcione, 1992). Data are reported in Figs. 1 and 2 and show how complex the energy distribution among different modes can be (see also Dal Moro, 2010a; O'Neill et al., 2004; O'Neill and Matsuoka, 2005). For the first case (Fig. 1) fundamental and first higher modes merge together thus simulating a signal that would be easily misinterpreted as a single mode. Example reported in Fig. 2 shows the presence of the fundamental mode only up to about 33 Hz. The signal between 35 and 52 Hz actually pertain to the second higher mode while the energy for frequencies higher than about 52 Hz is basically related to the first higher mode.

Problems are particularly severe when, due to the site characteristics and the acquisition setting, different modes coalesce into a unique signal that inevitably results hard to interpret (see for instance

E-mail address: g_dal_moro@hotmail.com.

0926-9851/$ – see front matter © 2010 Elsevier B.V. All rights reserved.
doi:10.1016/j.jappgeo.2010.08.004

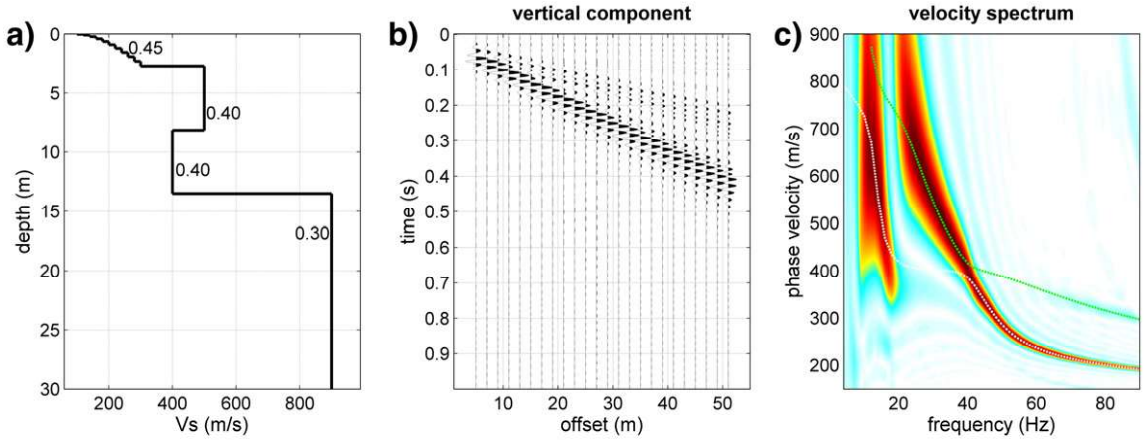

Fig. 1. Synthetic dataset showing an example of complex mode interlacing: a) V_S model (reported numbers represent the adopted Poisson values); b) seismic traces for the vertical component (vertical impact source); c) computed velocity spectrum with overlapped the theoretical Rayleigh-wave dispersion curves for the first 2 modes.

Fig. 1). The simplistic assumptions that fundamental mode is the most energetic and/or that higher modes appear typically at higher frequencies often result in severe mistakes in velocity spectra interpretation, thus leading to erroneous V_S profiles (see Fig. 3 for a field *MASW* dataset).

Furthermore, a typical source of misleading signals may be also represented by guided waves that may sometimes generate very high amplitude signals with dispersive character (e.g. Robertsson et al., 1995; Roth and Holliger, 1999).

Reported data clearly show how complex and seemingly puzzling energy distribution can actually be. It results consequently apparent that the common practice of picking maxima in the *f-k* or *v-f* domain and consider them as related to simple mode distributions (very often it is assumed that most of the energy pertains to the fundamental mode) can lead to severe mistakes in the retrieved V_S profile. On the other side, when properly interpreted, higher modes provide valuable information about the actual model, highly reducing the non-uniqueness of the solution (Dal Moro, 2010b). It should be then properly acknowledged that velocity spectra interpretation is a task that must be tackled very cautiously also considering that any kind of automatic procedure now and then proposed for SW analysis or inversion is necessarily based on assumptions that, even though valid under some circumstances, cannot be universally generalized.

On the other side, Horizontal-to-Vertical Spectral Ratio (*HVSR*) has been traditionally used for determining site resonance frequency (Nakamura, 1989, 1996, 2000) but more recently some authors attempted to use it as contributory tool for retrieving information about vertical V_S profile (e.g. Fäh et al., 2003). The main problem with *HVSR* is the unclear and highly debated physical model to adopt for its modelling. Relative contribution of Rayleigh Love and body waves is an "unsolvable" problem as the relationships vary with the frequencies and is clearly site-dependant (Fäh et al., 2001; Bonnefoy-Claudet et al., 2008). Furthermore the contribution of the number of modes while considering the surface wave contribution and the influence of quality factors are further problems (Lunedei and Albarello, 2009; Albarello and Lunedei, 2010) as also the severe non-uniqueness of the solution (Fig. 4). This latter problem is basically due to the fact that *HVSR* is sensitive to V_S contrasts and not to absolute V_S values. Further sources of problems are related to the possible presence of anthropic components and the stability and statistical robustness of average *HVSR*.

All of these problems eventually prevent *HVSR* from being a fully stand-alone solution for V_S profiling.

Given such a scenario, an efficient joint inversion tool capable of overcoming problems and limits of both methodologies and provides a reliable subsurface model is clearly highly desirable.

When a problem involves the minimization of two or more objectives, the standard approach is represented by a normalized summation that provides a single-objective able to account for the typically different nature and magnitude of the considered phenomena. A single cost function is consequently obtained and the minimization problem is then performed through standard solvers.

Such approach is often problematic not only because of the mathematically and physically inelegant summation of quantities with different magnitudes and units of measurements (in our case m/s for the dispersion curve and the unitless Horizontal-to-Vertical

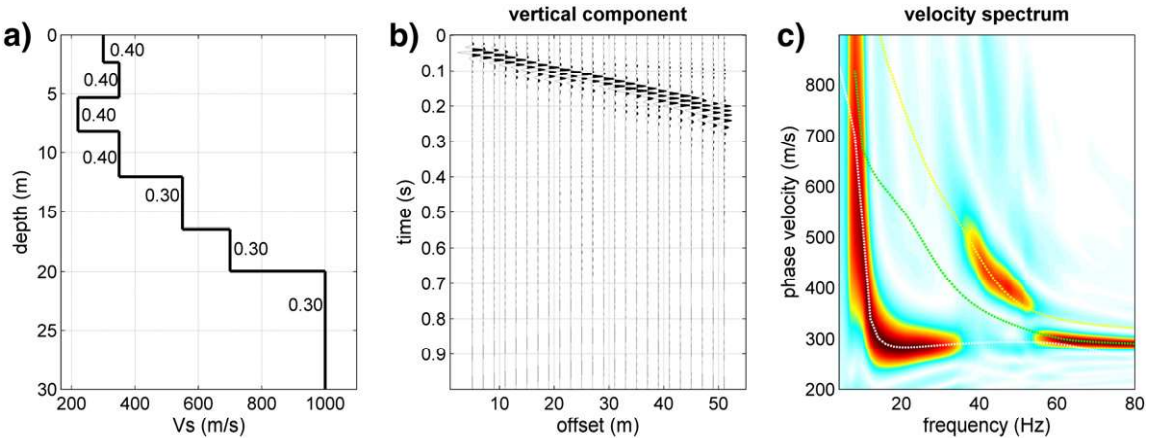

Fig. 2. Synthetic dataset showing a further example of complex mode interlacing: a) V_S model (reported numbers represent the adopted Poisson values); b) seismic traces for the vertical component (vertical impact source); and c) computed velocity spectrum with overlapped the theoretical Rayleigh-wave dispersion curves for the first 3 modes.

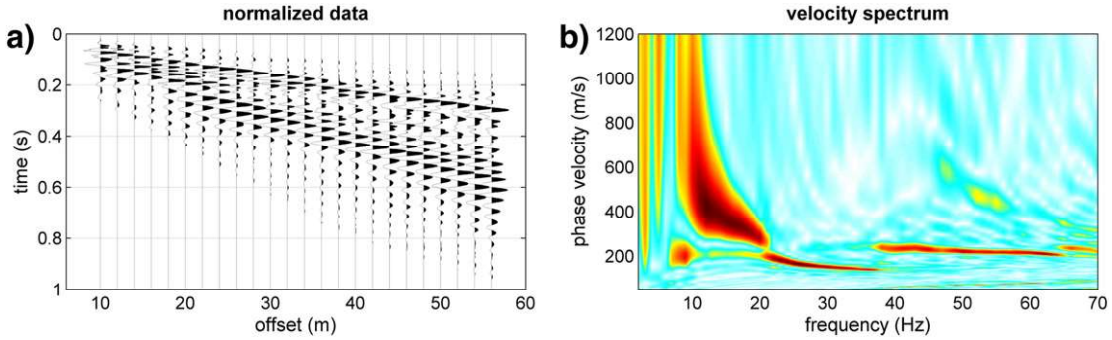

Fig. 3. *MASW* field dataset: acquired traces (vertical component and vertical sledgehammer impact) and computed velocity spectrum. Several mode jumps are apparent.

Spectral Ratio). The critical point is indeed represented by the bad performances that such approach implies when dealing with problems characterized by high non-uniqueness and the impossibility to eventually assess the goodness of the retrieved model(s) in a rigorous way. In fact, using a single cost function results in the impossibility of evaluating the actual validity of the retrieved model. Some minimum will be necessarily reached but there is no way to evaluate the overall congruency of the designed and parametrized inversion (and retrieved models). This is a particularly heavy problem especially when the objectives are characterized by several local minima. In this respect SW dispersion curves and *HVSR* are two extremely tricky functionals as both suffer from intrinsic non-uniqueness and data interpretation problems. Their joint inversion through standard single-objective genetic procedures has already been faced by some author. Here we present a joint inversion carried out through a Multi-Objective Evolutionary Algorithm (MOEA) exploiting the Pareto dominance criterion (Van Van Veldhuizen and Lamont, 1998a,b, 2000; Dal Moro and Pipan, 2007; Dal Moro, 2008).

A number of synthetic cases were considered to evaluate the behavior of the cost functions under different assumptions. Eventually a field dataset is analyzed and discussed.

2. Adopted approach

A general overview on MOEAs is given by several authors (Fonseca and Fleming, 1993; Van Veldhuizen and Lamont, 1998a,b, 2000; Coello Coello, 2003) while their application for joint seismic-data analysis is presented in Dal Moro and Pipan (2007) and Dal Moro (2008).

A comprehensive exposition of the ideas and principia would then result redundant and solely the basic points are here recalled.

The general outline is actually quite simple. An initial model population is (typically randomly) set and the evolutionary process is determined by the usual basic operations: *selection*, *crossover* and *mutation*. The characterizing point is represented by the way *selection* is accomplished.

The need of keeping separate the two objectives (thus defining a *Multi-Objective Problem* — MOP) prevents us from using the simple standard and intuitive rule adopted for single-objective problems that states that *the smaller the misfit the fittest the model*.

A correct solution is provided by the Pareto criterion: a model is given a rank (then used for the *selection* procedure) according to the number of models that *dominate* it.

A vector $\vec{u} = (u_1, u_2, ..., u_k)$ is said to dominate $\vec{v} = (v_1, v_2, ..., v_k)$ if and only if $\vec{u}$ is partially less than $\vec{v}$, that is:

$$\forall i \in \{1, ..., k\}, u_i \leq v_i \wedge \exists i \in \{1, ..., k\}: u_i < v_i \quad (1)$$

where k represents the number of considered objective functions.

The Pareto models are thus such that no improvement in one objective function can be obtained without a deterioration of at least one of the other objective functions.

A solution $x \in \Omega$ (the decision variable space) is then said to be *Pareto optimal* with respect to the universe Ω if and only if there is no $x' \in \Omega$ for which $\vec{v} = F(x')$ dominates $\vec{u} = F(x)$.

Eventually, at the end of the optimization procedure among all the evaluated models a subset of undominated models is identified. Such subset determines the so-called *Pareto front* which is our final

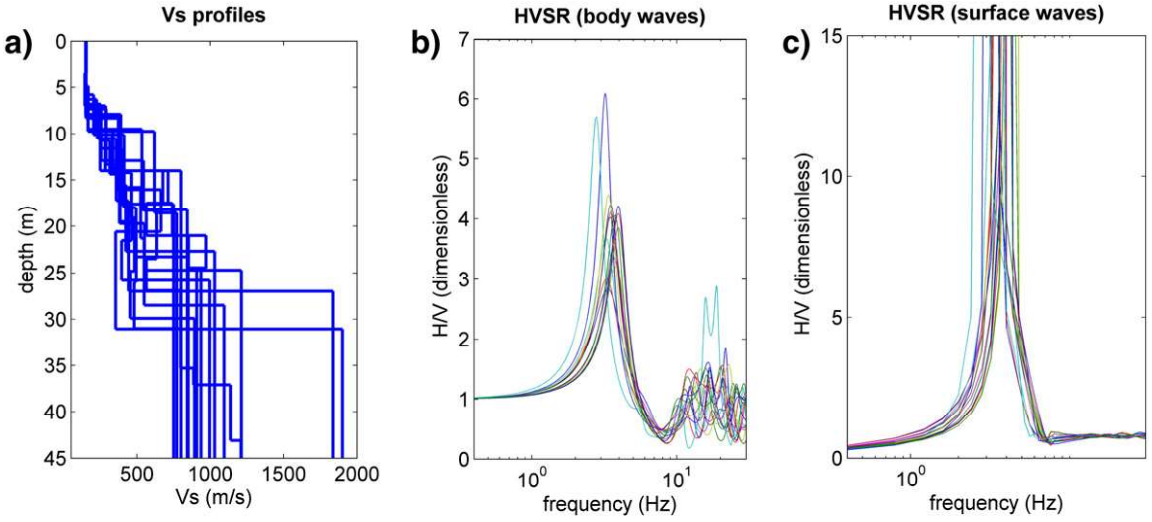

Fig. 4. *HVSR* computed for the reported models (a) both according to body waves (Herak, 2008) (b) and surface-wave ellipticity (Lunedei and Albarello, 2009) and (c): non-uniqueness of the solution is apparent.

solution. Please notice that typically, MOEAs do not provide a single solution/model but rather a set of models which, in terms of Pareto optimality, must be considered equivalent as all of them are undominated.

Of course, for practical uses, they could be averaged into a single mean model but this would be an arbitrary operation as in a MOP prospective they are all absolutely equivalent in terms of goodness.

As shown in Dal Moro and Pipan (2007) and Dal Moro (2008) the symmetry of the Pareto front models with respect to the universe of the evaluated models is a key index able to put in evidence the overall goodness of the inversion process, preliminary assumptions and data interpretations (Fig. 5).

2.1. Joint Inversions via MOEA

In the current case the two objective functions to minimize are represented by two misfits, the first one related to Rayleigh-wave dispersion curves and the second one to *HVSR*.

Rayleigh-wave dispersion curves were defined according to Dunkin (1965) while *HVSR* were calculated considering SW ellipticity according to Lunedei and Albarello (2009) — thus taking into account multimodes and quality factors as well.

Adopted genetic parameters for all the analyzed cases (synthetic and field datasets) are reported in Table 1 (in order to simulate ordinary procedures thus avoiding high computational times, population size and number of generations were fixed to reasonable values).

The two considered objective functions were defined as the *root-mean-square* (*rms*) misfit between the observed and calculated dispersion curves (hereafter obj#1) and *HVSR* (hereafter obj#2):

$$obj = \sqrt{\frac{\sum_{i=1}^{n}\left(\Phi_{obs_i} - \Phi_{cal_i}\right)^2}{n}} \tag{2}$$

where Φ represents the Rayleigh-wave phase velocities (obj#1) or *HVSR* (obj#2) and n is the number of points for the given objective.

In order to avoid that higher misfits occurring at the lower frequencies dominate over the smaller misfits of the higher frequencies (possibly determining a loss of resolution for the shallowest layers), a frequency-dependant weighting factor is adopted for the dispersion curve misfit:

$$w_i = \sqrt{\frac{f_i}{f_M}} \tag{3}$$

where f_M represents the maximum frequency of the considered dispersion curve.

Table 1
Parameters adopted for the genetic optimization.

Population size	35
Crossover rate	0.75
Mutation rate	0.1
Number of generations	50

This kind of weighting has a twofold meaning in the context of the current joint analysis: on one side, for low frequencies dispersion curves have necessarily a higher uncertainty, on the other side it is well-known that *HVSR* is extremely sensitive to deep V_S variations. As a consequence the general idea which lies behind the joint analysis of dispersion curves and *HVSR* is that dispersion curves represent the constrains (especially for the shallowest layers) necessary to confine and exploit the information "hidden" in the *HVSR* in particular with respect to the deepest structure.

3. Synthetic data

Similar to the approach followed in Dal Moro and Pipan (2007) and Dal Moro (2008), we evaluated the proposed methodology by comparing results obtained while adopting proper and incorrect assumptions. For the sake of brevity we will present only few representative cases summarized in Table 2.

The reference synthetic model is summarized in Table 3 (the Vs30 value – defined according to the well-known $Vs30 = 30/\mathrm{sum}(h_i/V_{Si})$ equation – is here reported only to synthetically summarize the overall model characteristics). Dispersion and H/V curves were considered in the 5–50 and 0.4–25 Hz range respectively. For the computation of *HVSR* four modes were adopted. Q_S values were fixed according to the rule of thumb $Q_S = V_S/10$, while $Q_P = 2Q_S$.

During the joint inversion Poisson ratio was free to vary in the 0.35–0.31 range, while the number of modes to use in the *HVSR* computation between 1 (fundamental mode only) and 7.

The first case (case#1) represents a very well-determined situation: the number of layers assumed during the inversion procedure is the same as the reference synthetic model (5 layers).

The second case (case#2) is meant as an over-parametrization of the inversion process: 7 layers are adopted (instead of 5).

The third case represents a possible source of problems: *HVSR* is modeled according to SW ellipticity but without taking into consideration attenuation and higher modes — see Lunedei and Albarello (2009) for theoretical aspects and Dal Moro (2010a) for a case study. While *HVSR* for the reference model (Table 3) was computed considering attenuation ($Q_S = V_S/10$) and 4 modes, in case#3 the modelling during the joint inversion is based on fundamental mode only and no attenuation is considered (purely elastic case).

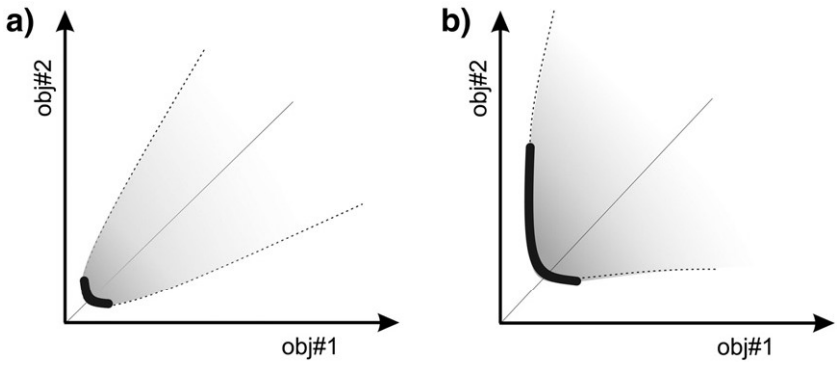

Fig. 5. Pareto front: a) symmetric distribution of the Pareto front models as evidence of a properly accomplished inversion; and b) asymmetric distribution of the Pareto front models as a consequence of relevant inconsistencies in the inversion procedure (see Dal Moro and Pipan, 2007; Dal Moro, 2008).

Table 2
Summary table of the considered cases.

Case	Description
#1	Proper number of layers (5).
#2	Higher number of layers (7).
#3	Purely elastic *HVSR* modelling with fundamental mode only.
#4	Major problem: erroneous data interpretation and/or severe lateral variations.

Last case (case#4) can be considered as representative of major inconsistencies between the two objectives. Considered dispersion curve is based on the model reported in Table 3 while *HVSR* refers to the model in Table 4.

As the incongruence is purely relative, the error can be considered as due to any of the considered objectives: erroneous picking of the dispersion curve, presence of anthropic components in the *HVSR* or non-representative *HVSR* amplitudes related to statistical microtremor variability.

It is well-know that dispersion curve analysis necessarily provides a kind of average vertical V_S profile along the array length (thus several tens of meters) while *HVSR* results sensitive to very local conditions thus evidencing possible significant lateral variations. As a consequence, in areas where non-negligible lateral variations occur, the two models (one pertinent to the dispersion curve and the other to *HVSR*) are somehow different and case#4 can then be also considered as representative of a condition where major lateral variations occur.

Surface wave dispersion analysis via *MASW* allows an extremely precise determination of V_S values in the shallowest layers (approximately down to 5–10 m), while precision decreases for deeper layers. That means that by analyzing dispersion curves only, it is possible to narrow the search space to adopt for the shallowest layer(s) in the joint inversion. This is way the search space adopted for the shallowest layer during the joint inversion is relatively (see background area in the retrieved models in Figs. 6b–10b).

3.1. Case#1

The consistency of the adopted assumptions with respect to the reference model mirrors in a pointy distribution of the models in the objective space and in a symmetrical distribution of the Pareto front models with respect to the rest of the computed models (Fig. 6a). Computed and reference dispersion and H/V curves appear overall consistent (Fig. 6c and d) (Vs30 values of the Pareto front models range between 244 and 248 m/s thus perfectly matching the Vs30 value of the reference model).

3.2. Case#2

The over-parametrization of the joint inversion produces some minor deviations from the ideal case (compare Fig. 7a with Figs. 5a and 6a). Model distribution in the objective space is still pointy (Fig. 7a) but the Pareto front symmetry is lost. Please notice that the overall fitting of both dispersion and H/V curves is still quite good (Fig. 7c and d), thus demonstrating the severe non-uniqueness of both objective functions

Table 3
Considered synthetic model: Poisson values 0.33, Vs30 = 247 m/s, density fixed according to Gardner et al. (1974).

Thickness (m)	V_S (m/s)
2	120
4	180
10	250
20	330
Half space	440

Table 4
Synthetic model adopted for the dispersion curve used for the case#4: Poisson values 0.33, Vs30 = 378 m/s, density fixed according to Gardner et al. (1974).

Thickness (m)	V_S (m/s)
1	150
3	210
7	330
10	450
Half space	600

(Vs30 values of the retrieved models range between 250 and 255 m/s, thus still close to the 247 m/s value of the reference model).

As the larger number of layers means a higher degree of freedom of the system, it was conjectured that such minor deviation from a perfectly idealized outcome was due to an insufficient number of models (i.e. population size) and generations (see Table 1) during the heuristic optimization. A further inversion was thus performed while increasing these parameters to 50 and 70 respectively. Results reported in Fig. 8 would actually confirm such interpretation (as expected the Pareto front models are now symmetric). Vs30 values range between 248 and 256 m/s.

Please notice that the variability of the final Pareto front models is larger as depth increases and expresses the uncertainty of the final model (clearly related to the non-uniqueness of the solution).

3.3. Case#3

As a result of inappropriate *HVSR* modelling the Pareto front asymmetry (see Fig. 9a) result is now quite severe, although the overall congruency of dispersion and H/V curves appear somehow acceptable (Vs30 values of the final Pareto front models range between 241 and 248 m/s) thus showing the ability of Pareto front evaluation of highlighting inconsistencies otherwise not easily put in evidence. Please notice that while retrieved models are quite in agreement with the reference one, the Pareto front asymmetry shows the inconsistency due to the inappropriate *HVSR* modelling assumptions (fundamental mode only and no attenuation).

It is noteworthy to remark that the role of attenuation and higher modes in *HVSR* modelling fundamentally reflects in a kind of scaling factor (their inclusion generally determines a decrease of the amplitude of the peaks — see Lunedei and Albarello, 2009). The reported results seem to show that the inclusion of attenuation and higher modes in the *HVSR* modelling performed in the framework of a Pareto-based optimization might (at least in some cases) not be vital for the proper identification of the final models(s).

This is actually reasonable because although actual *HVSR* amplitudes are not properly reproduced, what actually matters is the position (i.e. the frequency) of the peak(s).

Such results will be also useful during the analyses of the field dataset and will be a key point while discussing the overall outcomes of the current study.

3.4. Case#4

In this final case (see Fig. 10) the entire set of outcomes (model distribution in the objective space, the Pareto front asymmetry, inconsistency between the dispersion and H/V curves of the Pareto front models) shows clear evidence of major problems also indicated by a very wide range of the final Pareto front models synthesized by Vs30 values ranging between 318 and 401 m/s.

4. Field dataset

Considered dataset was acquired on a land reclamation zone (soft sediments lying over a massive calcarenite) on a foothill area in NE

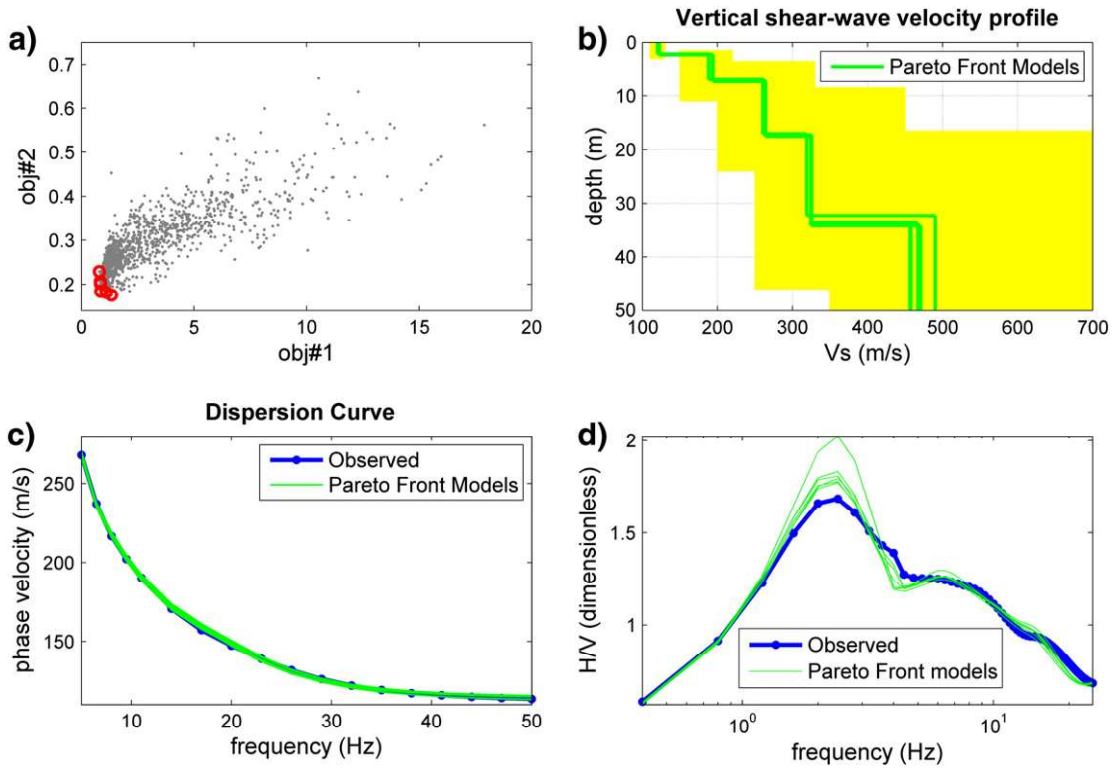

Fig. 6. *Case#1*. Main outcomes of performed joint inversion: a) models in the objective space (circles highlight the Pareto front models); b) V_S profiles for the Pareto front models (colored area in the background represents the adopted search space); c) reference and retrieved dispersion curves (Pareto front models); and d) reference and retrieved *HVSR* (Pareto front models).

Italy. In Fig. 11 are reported acquired seismic data (*MASW*) together with the computed velocity spectrum, while observed *HSVR* (considering 20-minute long acquisition) is shown in Fig. 12.

Preliminary Rayleigh-wave dispersion and attenuation analyses (e.g. Xia et al., 2002; Dal Moro, 2010a) were performed in order to retrieve V_S values for the shallowest layers (thus also being able to fix

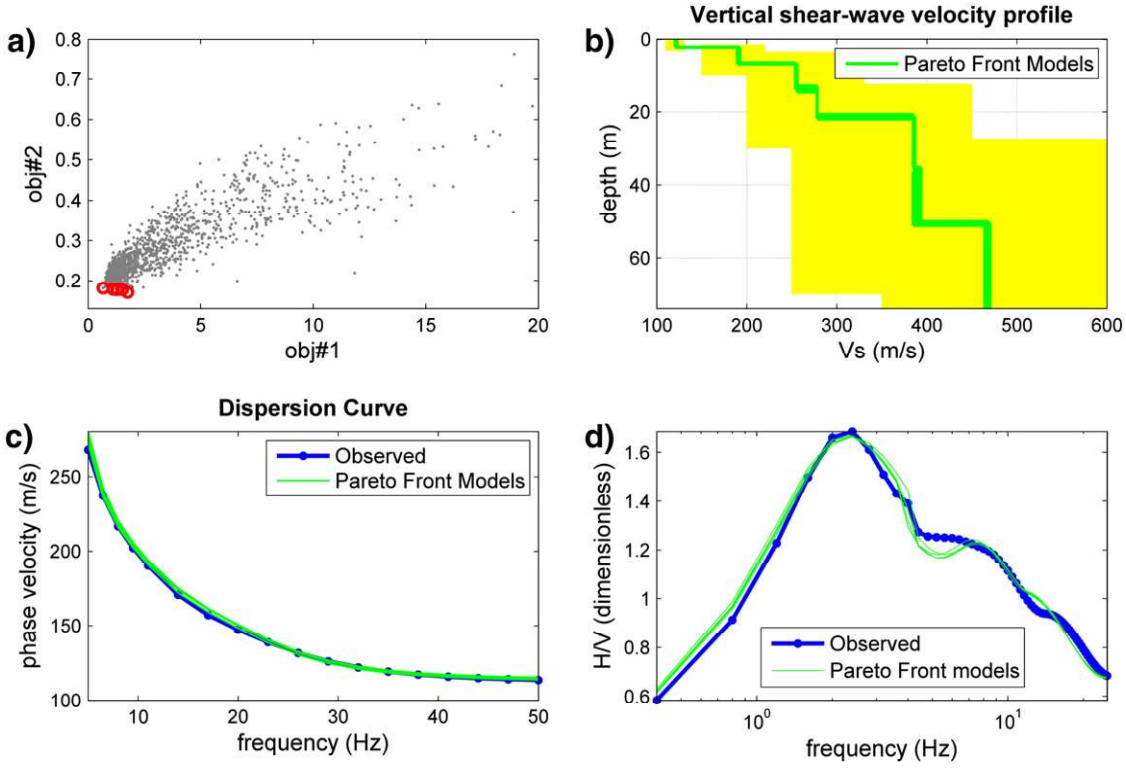

Fig. 7. *Case#2*. Main outcomes of performed joint inversion: a) models in the objective space (circles highlight the Pareto front models); b) V_S profiles for the Pareto front models (colored area in the background represents the adopted search space); c) reference and retrieved dispersion curves (Pareto front models); and d) reference and retrieved *HVSR* (Pareto front models).

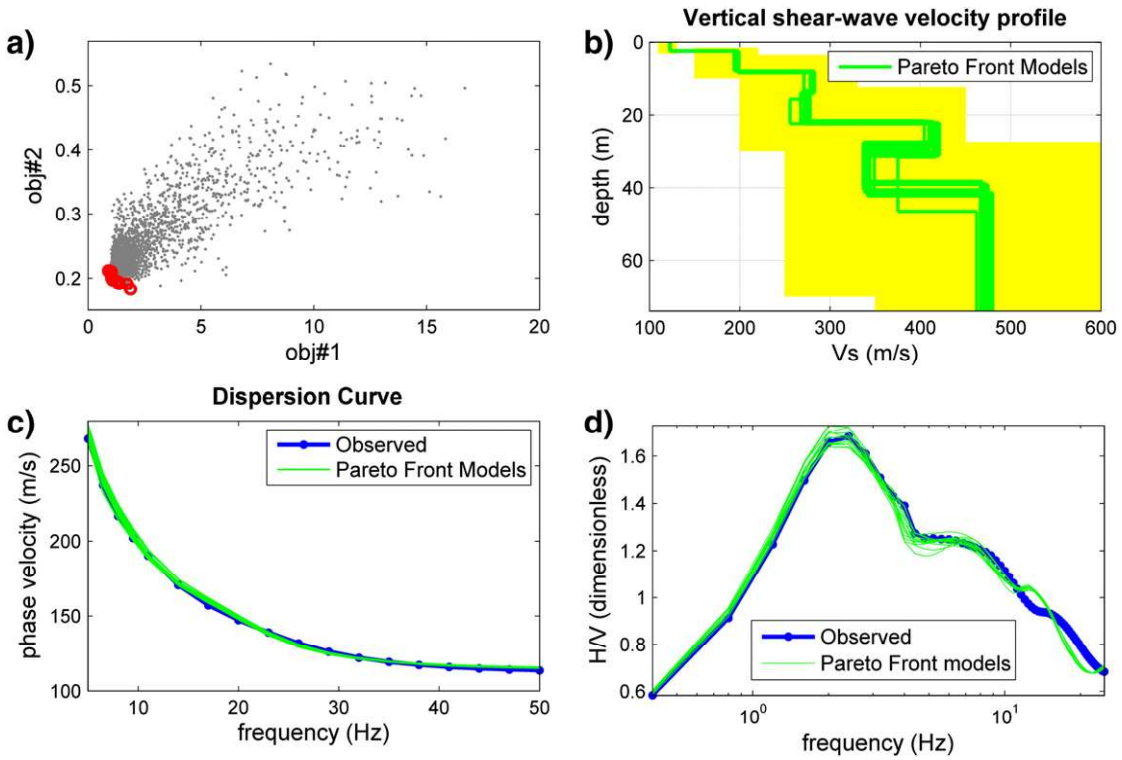

Fig. 8. *Case#2*. Main outcomes of performed joint inversion while considering model population 50 and generation number 70: a) models in the objective space (circles highlight the Pareto front models); b) V_S profiles for the Pareto front models (colored area in the background represents the adopted search space); c) reference and retrieved dispersion curves (Pareto front models); and d) reference and retrieved *HVSR* (Pareto front models).

a reasonable search space for the final joint analysis) and evaluate soft-sediment quality factors Q_S. Results are presented in Fig. 13 and clearly show a monotonous sequence of soft sediments down to a depth of approximately 20 m. Please notice that, since the aim was to exploit the complementary information provided by SWs and *HVSR* for shallower and deeper layers respectively, dispersion curve was

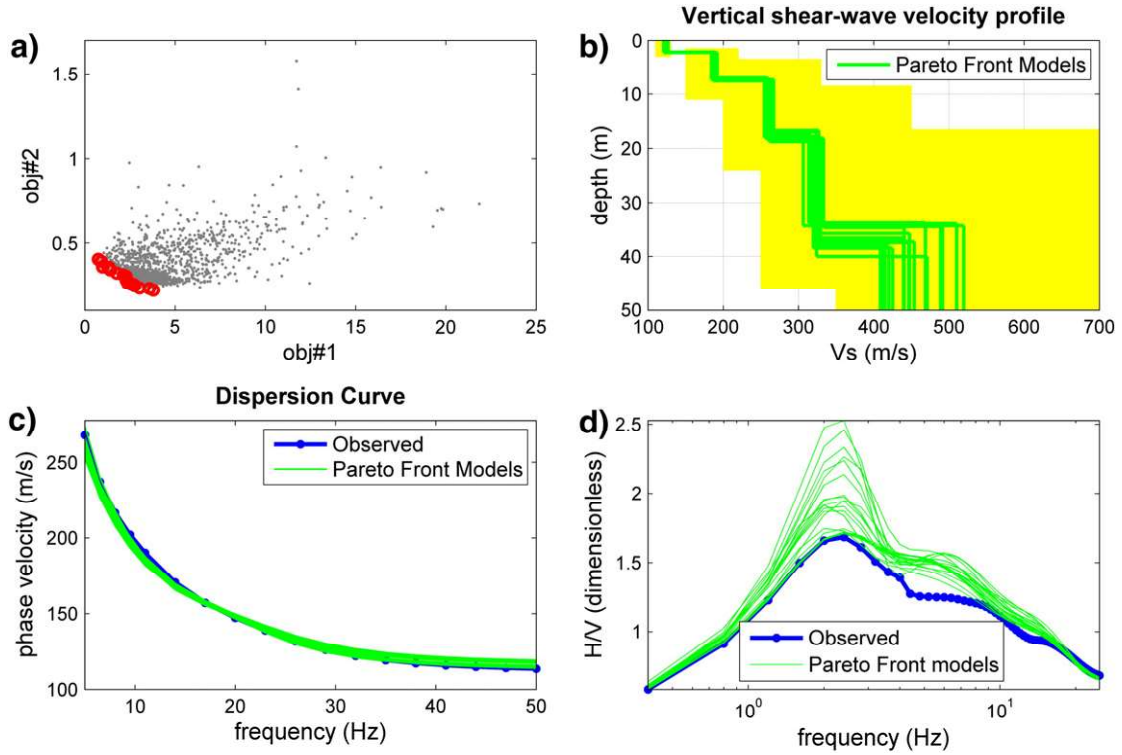

Fig. 9. *Case#3*. Main outcomes of performed joint inversion: a) models in the objective space (circles highlight the Pareto front models); b) V_S profiles for the Pareto front models (colored area in the background represents the adopted search space); c) reference and retrieved dispersion curves (Pareto front models); and d) reference and retrieved *HVSR* (Pareto front models).

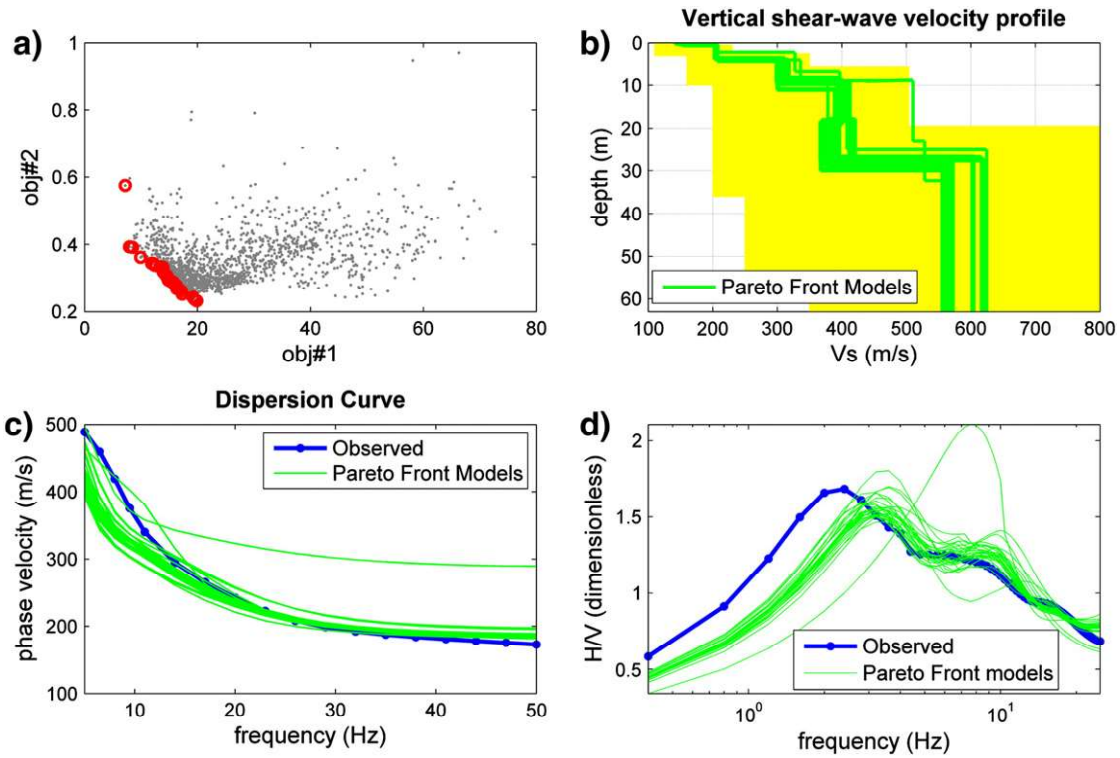

Fig. 10. *Case#4*. Main outcomes of performed joint inversion: a) models in the objective space (circles highlight the Pareto front models); b) V_S profiles for the Pareto front models (light-colored area in the background represents the adopted search space); c) reference and retrieved dispersion curves (Pareto front models); and d) reference and retrieved *HVSR* (Pareto front models).

picked in a very cautious and conservative way (i.e. not considering frequencies lower than about 5 Hz), as we wished not to jeopardize the inversion procedure with possible inaccurate low-frequency picks.

Q_S values for the soft sediments result around 20 thus allowing to depict an approximate $Q_S = V_S/6$ relationship. Please notice that for low V_S/V_P ratios (i.e. high Poisson values) Q_P has a minor effect on Rayleigh-wave attenuation (Xia et al., 2002) and sensitivity analyses show that it is quite hard to discriminate Q values for high-quality rock materials (White, 1992) — so Q values for the underlying calcarenite are necessarily poorly defined.

These preliminary results were then considered for setting a reasonable search space and fixing V_S-Q_S general relation to adopt for the joint inversion. Please notice that considering Q values as an independent variable would be both possible and practically useless for at least two reasons:

1. Their values were initially determined through the Rayleigh-wave attenuation analysis (Fig. 13) while in order to avoid a useless increase in the number of variables, their values during the joint inversion where linked to the shear-wave velocities according to the above-reported relationship;
2. Possible residual influence of quality factors on *HVSR* (specifically on the amplitudes of the peaks) is somehow accounted by the fact that the number of modes considered while computing *HVSR* is a variable (compare Lunedei and Albarello, 2009; Albarello and Lunedei, 2010; Dal Moro, 2010a).

The large V_S contrast due to the contact between the superficial soft sediments and the calcarenite bedrock can determine relevant computational problems while considering *HVSR* computation via SW ellipticity. For those who deal with H/V modelling only, this well-known problem is often surmounted by adding further layers to get a smoother transition which would eventually overcome numerical instabilities.

In Fig. 14 we present the results of the inversion performed while considering the indicated search space (background area in Fig. 14b). Vs30 values of the Pareto front models range between 202 and 222 m/s. It is apparent the very high amplitude of the computed H/V curves clearly due to the dramatic V_S contrast between the soft sediment and

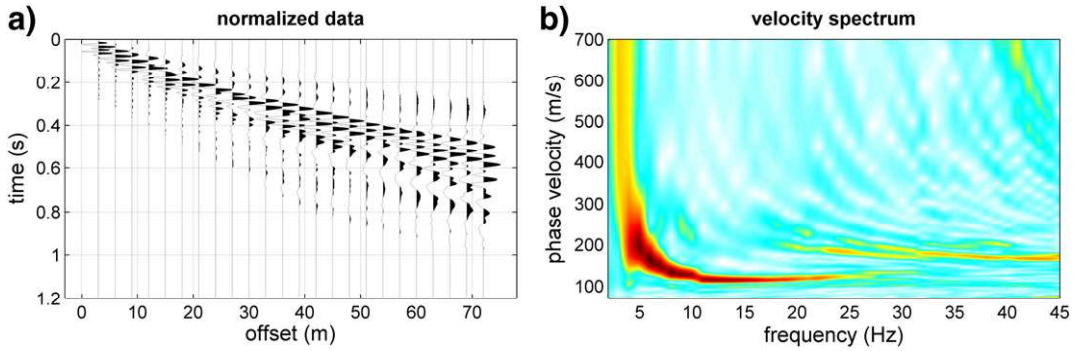

Fig. 11. Field dataset. Acquired multi-channel seismic data: a) x-t domain and b) velocity spectrum.

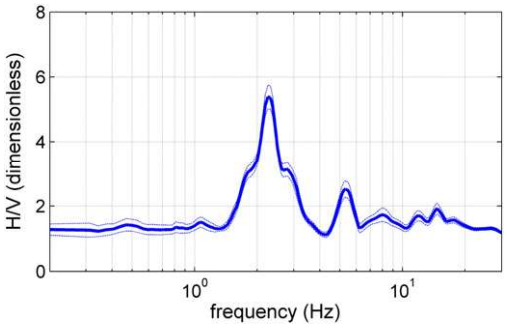

Fig. 12. Field dataset. Observed H/V spectral ratio.

the calcarenite bedrock. It must be also mentioned that different *HVSR* measurements were performed on the area with different equipment, at various time and in different periods of the year. Results showed a certain variability in the amplitude of the main peak thus also giving evidence of some problematic aspects related to the statistical robustness of *HVSR* measurements (details about these aspects would go behind the goal of the current paper).

Although most of the authors agree that surface-wave contribution to *HVSR* is essential it is also clear that, especially for the fundamental period, *HVSR* from body waves (Herak, 2008) can, at least under some circumstances, represent a better approximation — see Albarello and Lunedei (2010) for a discussion about this point.

Results obtained while adopting this approach (Herak, 2008) are presented in Fig. 15 (Vs30 values of the Pareto front models range between 205 and 214 m/s). It is possible to notice that the main peak (the resonance frequency) is now properly represented while the H/V peaks at higher frequencies are not (compare also Fig. 4b and c). Such high-frequency peaks are typically not present in field data and can be interpreted as one of the evidences of the predominant role of SW ellipticity at high frequency. On the other side the very good fitting for the main peak determined by the body wave approximation at the resonance frequency (in this case about 2.5 Hz) supports the idea of Albarello and Lunedei (2010), which is actually a kind of compromise between those who support the predominance of surface waves and those who think of body waves as driving force in *HVSR*: when a clear and dominant peak due to a major lithological contact (as in the present case) is present, body wave approximation might be considered as a good approximation. Please notice the overall congruency of the outcomes presented in Fig. 15.

5. Discussion

The results of the analyses performed while considering the Pareto optimality both on synthetic and field datasets suggested to briefly investigate the properties and meaning of the Pareto front with respect to the nature of the two objective functions — see also Dal Moro and Pipan (2007) and Dal Moro (2008).

In order to highlight the meaning of the model distribution in the objective space and the asymmetry of the Pareto front models, two functions with peculiar characteristics were considered (Figs. 16 and 17). In such simulation x1 and x2 represent the independent variables (i.e. the parameters of the problem) and z the objective. While obj#1 has a single minimum, obj#2 has also several local minima. In order to simulate a certain inconsistency of the two objectives the two global minima were fixed at 2 slightly different positions (see close up in Fig. 16c). A small amount of random noise is also added.

As predictable, model distribution in the objective space (Fig. 17) tends to bend towards the x-axis due to the fact that small objective values are more numerous for obj#2.

Furthermore, the asymmetric distributions of the Pareto front models due to the inconsistency of the two functions (the global minima do not occur at the same location) give further and specific evidence of this tendency.

This simple simulation can be helpful to justify why and how model distribution in the objective space (Pareto front models in particular) can (or tends to) deviate from a symmetric distribution.

In the joint inversion of SW dispersion curves and reflection/refraction travel times (Dal Moro and Pipan, 2007; Dal Moro, 2008)

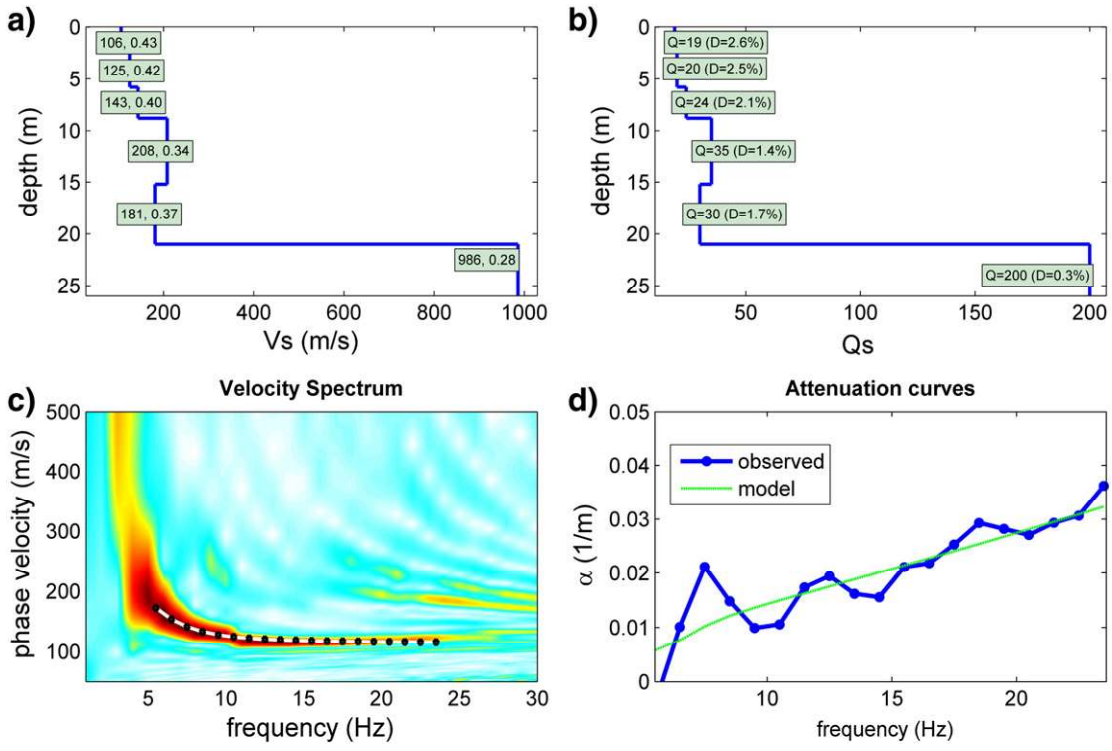

Fig. 13. Preliminary V_S and Q_S values retrieved from Rayleigh wave dispersion and attenuation analysis (see text).

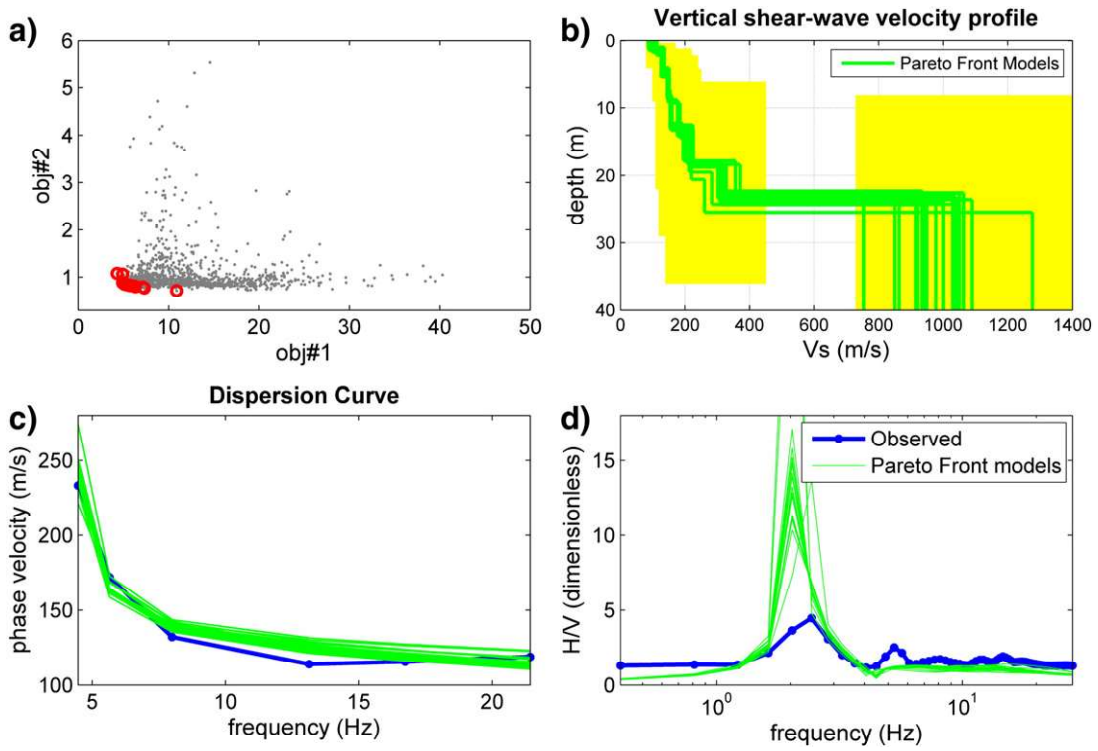

Fig. 14. Main outcomes of performed joint inversion while considering SW ellipticity: a) models in the objective space (circles highlight the Pareto front models); b) V_S profiles for the Pareto front models (colored area in the background represents the adopted search space); c) reference and retrieved dispersion curves (Pareto front models); and d) reference and retrieved *HVSR* (Pareto front models).

it was observed that in case of incorrect inversion parametrization the Pareto front models invariably tend to move towards the axis representing the reflection/refraction misfit. On the other side, in the present case Pareto front tends to align along the axis representing the dispersion curve misfit rather than the *HVSR* misfit (see e.g. Fig. 9).

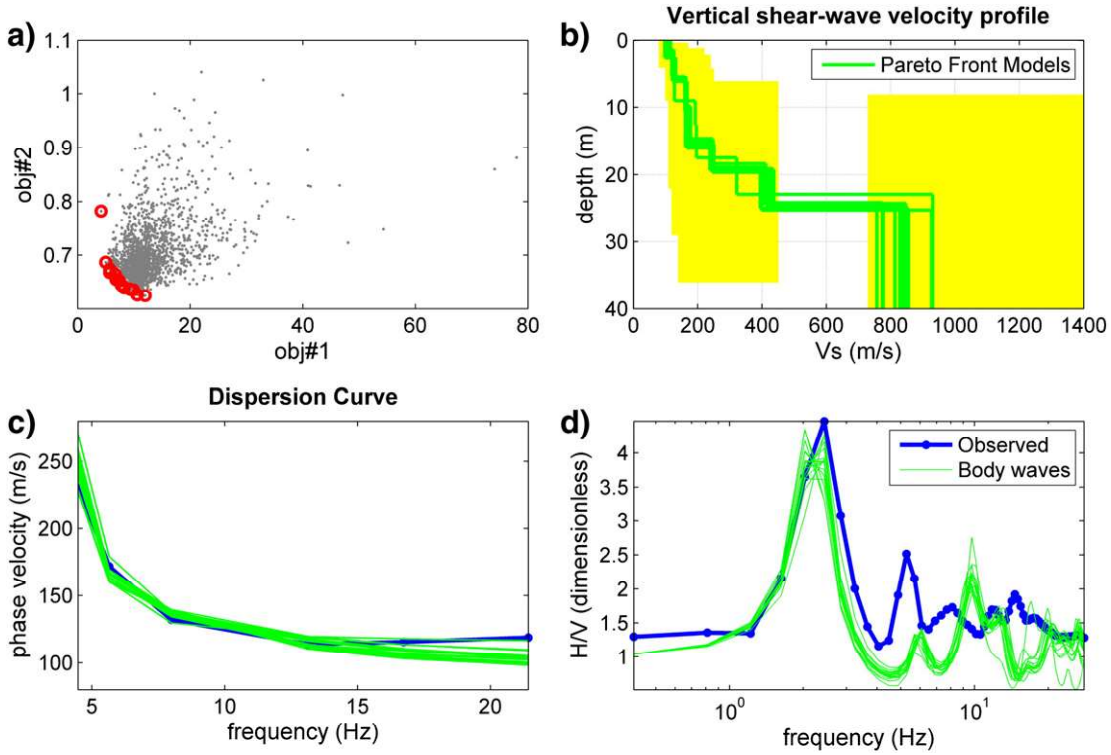

Fig. 15. Main outcomes of performed joint inversion while considering *HVSR* from body waves: a) models in the objective space (circles highlight the Pareto front models); b) V_S profiles for the Pareto front models (colored area in the background represents the adopted search space); c) reference and retrieved dispersion curves (Pareto front models); and d) reference and retrieved *HVSR* (Pareto front models).

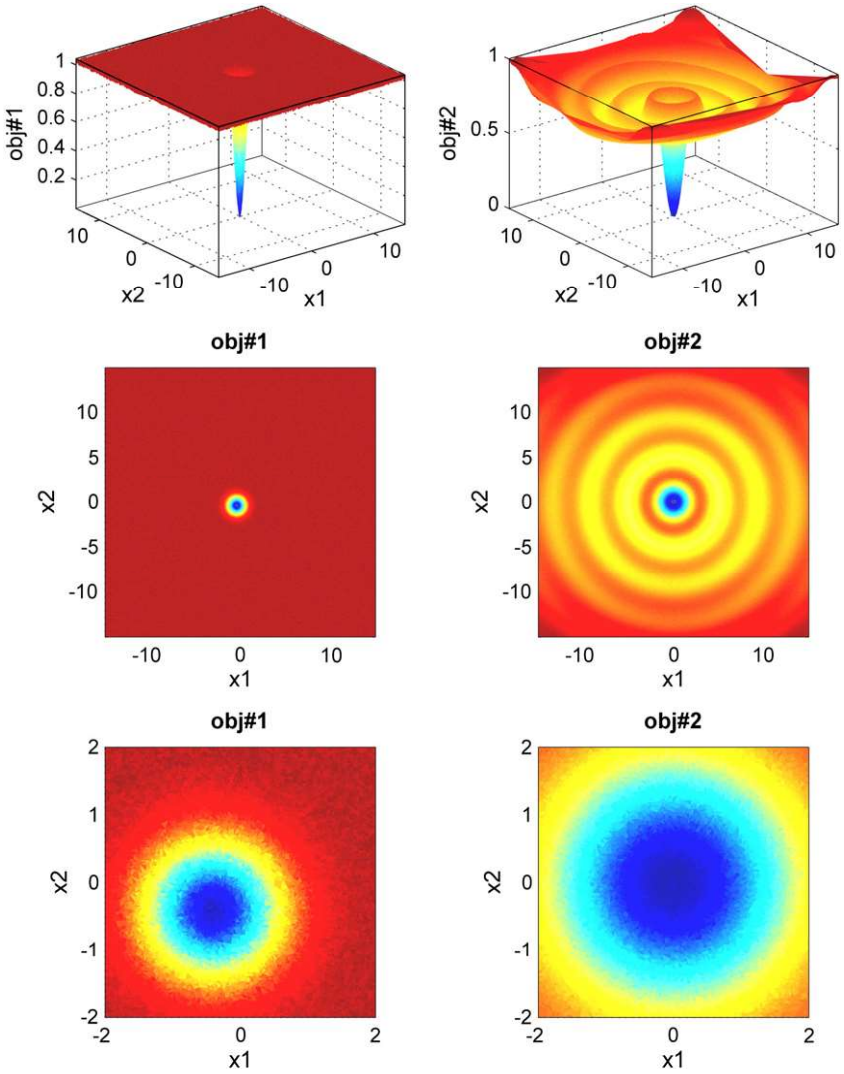

Fig. 16. Two functions with different characteristics: single-minimum function (obj#1) on the left and several local minima function (obj#2) on the right (upper panel 3D view, intermediate panel 2D contour map, lower panel close up of the 2D contour map). Please notice that the two minima have slightly different x1–x2 coordinates.

In the light of the previously reported numerical simulations, the reason for such different behavior can be sought in the different so-to-say degree of non-uniqueness (i.e. the number of minima) of the considered objectives.

For the previously analyzed cases (dispersion curves and reflection/refraction travel times) models distribution in the objective space demonstrated an higher degree of non-uniqueness for the dispersion curve inversion while in the present case non-uniqueness related to *HVSR* appears somehow more severe than that associated to dispersion curves.

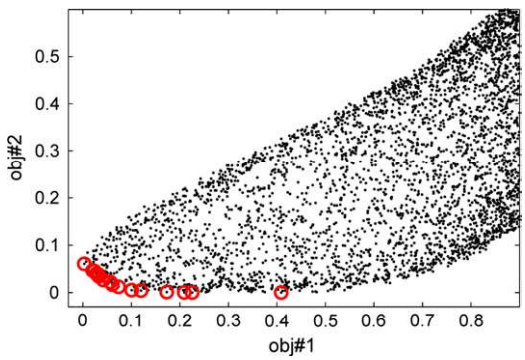

Fig. 17. Distribution of the two objective functions presented in Fig. 16. Notice how the model distribution tends to bend towards the x-axis (obj#1), due to the large number of local minima (i.e. small values) for the obj#2. Pareto front models (circles) further put in evidence this tendency.

6. Conclusions

It is clear that, during SW dispersion curve analysis, erroneous or inaccurate velocity spectrum interpretation (due for instance to mode misidentification) necessarily leads to erroneous subsurface reconstruction. On the other side, due to its nature, *HVSR* is necessarily ambiguous, being that the action of V_S and thickness cannot be separated unless further data are involved (*HVSR* is defined by V_S contrasts and not by their absolute values).

Such scenario naturally leads to the idea of jointly inverting SW dispersion curves and *HVSR*.

The main advantage of keeping separate two (or more) objectives is related to the relevant added-value that is provided by the analysis of the distribution of the Pareto front models in the objective space.

Multi-objective Pareto-based analyses are in fact capable of revealing aspects that single-objective optimizers cannot image and highlight. As a matter of fact these latter can actually provide pointless final models representing a meaningless trade-off between the models singularly “preferred” by the two objective functions. Severe

non-uniqueness risks to furnish imprecise solutions as any inversion scheme based on a single cost function will necessarily lead to a minimum whose value and robustness cannot be evaluated.

In the present and previous studies (Dal Moro and Pipan, 2007; Dal Moro, 2008), Pareto optimality is adopted not only as a ranking system for genetic procedures but also as a tool able to provide few indices (symmetry, coherent decrease of objectives, etc.) related to the overall congruency of the performed inversion and consequently establish the goodness of the retrieved solution.

This reflects also in a kind of epistemic tool able to put in evidence possible inconsistencies in the modelling criteria (see e.g. data and comments related in particular to *case#3*).

As shown in the previous paragraph, model distribution in the objective space also furnishes an estimation of the relative non-uniqueness of the two objectives and variability of the Pareto front models show.

The analyses of the field dataset supports the idea that the *HVSR* peaks associate to the resonance frequency of the site is better expressed by the body wave approximation while at higher frequencies SW ellipticity should play the dominant role.

Acknowledgements

Part of the research was performed during the author's work at the University of Trieste (Italy). NICCOS (Italian Ministry of Foreign Affairs) and PRIN COFIN 2006 funds are acknowledged. The author is grateful to Prof. Dario Albarello and an anonymous reviewer for the helpful comments which definitely improved the paper.

References

Albarello, D., Lunedei, E., 2010. Alternative interpretations of horizontal to vertical spectral ratios of ambient vibrations: new insights from theoretical modeling. Bulletin of Earthquake Engineering 8, 519–534.

Bonnefoy-Claudet, S., Köhler, A., Cornou, C., Wathelet, M., Bard, P.-Y., 2008. Effects of love waves on microtremor H/V ratio. Bulletin of the Sismological Society of America 98, 288–300.

Carcione, J.M., 1992. Modeling anelastic singular surface waves in the Earth. Geophysics 57, 781–792.

Coello Coello, C.A., 2003. Guest editorial: special issue on evolutionary multiobjective optimization. IEEE Transactions on Evolutionary Computation 7, 97–99.

Dal Moro, G., 2008. V_S and V_P vertical profiling via joint inversion of Rayleigh waves and refraction travel times by means of bi-objective evolutionary algorithm. Journal of Applied Geophysics 66, 15–24.

Dal Moro, G., 2010a. Some Thorny Aspects about Surface Wave and HVSR Analyses: an Overview. Bollettino di Geofisica Teorica e Applicata, special issue, submitted.

Dal Moro, G., 2010b. Joint Analysis of Rayleigh and Love-wave Dispersion Curves: Issues, Criteria and Improvements. Shortly submitted to Pure and Applied Geophysics

Dal Moro, G., Pipan, M., 2007. Joint inversion of surface wave dispersion curves and reflection travel times via Multi-Objective Evolutionary Algorithms. Journal of Applied Geophysics 61, 56–81.

Dal Moro, G., Pipan, M., Gabrielli, P., 2007. Rayleigh wave dispersion curve inversion via genetic algorithms and marginal posterior probability density estimation. Journal of Applied Geophysics 61, 39–55.

Dunkin, J.W., 1965. Computation of model solutions in layered, elastic media at high frequencies. Bulletin of the Sismological Society of America 55, 335–358.

Evison, F.F., Orr, R.H., Ingham, C.E., 1959. Thickness of the earth's crust in Antarctica. Nature 183, 306–308.

Fäh, D., Kind, F., Giardini, D., 2001. A theoretical investigation of average H/V ratios. Geophysical Journal International 145, 535–549.

Fäh, D., Kind, F., Giardini, D., 2003. Inversion of local S-wave velocity structures from average H/V ratios, and their use for the estimation of site-effects. Journal of Seismology 7, 449–467.

Fonseca, C.M., Fleming, P.J., 1993. Genetic algorithms for multiobjective optimization: formulation, discussion and generalization. Proceeding of the fifth International Conference on Genetic Algorithms. Morgan-Kauffman, San Mateo, CA (USA), pp. 416–423.

Gardner, G.H.F., Gardner, L.W., Gregory, A.R., 1974. Formation velocity and density — the diagnostic basic for stratigraphic trap. Geophysics 39, 770–780.

Glangeaud, F., Mari, J., Lacoume, J.-L., Mars, J., Nardin, M., 1999. Dispersive seismic waves in geophysics. European Journal of Environmental and Engineering Geophysics 3, 265–306.

Herak, M., 2008. ModelHVSR — a Matlab tool to model horizontal-to-vertical spectral ratio of ambient noise. Computers and Geosciences 34, 1514–1526.

Ivanov, J., Miller, R.D., Xia, J., Steeples, D., Park, C.B., 2005a. The inverse problem of refraction traveltimes, part I: types of geophysical nonuniqueness through minimization. Pure and Applied Geophysics 162, 447–459.

Ivanov, J., Miller, R.D., Xia, J., Steeples, D., 2005b. The inverse problem of refraction traveltimes, part II: quantifying refraction nonuniqueness using a three-layer model. Pure and Applied Geophysics 162, 461–477.

Louie, J.N., 2001. Faster, better: shear-wave velocity to 100 meters depth from refraction microtremor arrays. Bulletin. Seismological Society of America 91, 347–364.

Luke, B., Calderón-Macías, C., Stone, R.C., Huynh, M., 2003. Nonuniqueness in inversion of seismic surface-wave data. Proceedings on the Symposium on the application of geophysics to engineering and environmental problems, Environmental and Engineering Geophysical Society, CD-ROMSUR05.

Lunedei, E., Albarello, D., 2009. On the seismic noise wavefield in a weakly dissipative layered Earth. Geophysical Journal International 177, 1001–1014.

Nakamura, Y., 1989. A method for dynamic characteristics estimation of subsurface using microtremor on the ground surface. Quarterly Report of Railway Technical Research Inst. (RTRI) 30, 25–33.

Nakamura, Y., 1996. Realtime Information Systems for Seismic Hazard Mitigation. Quarterly report of Railway Technical Research Inst. (RTRI) 37, 112–127.

Nakamura, Y., 2000. Clear identification of fundamental idea of Nakamura's technique and its applications. Proc XII World Conf. Earthquake Engineering, New Zealand, 2656.

O'Neill, A., Matsuoka, T., 2005. Dominant higher surface-wave modes and possible inversion pitfalls. Journal of Environmental and Engineering Geophysics 10, 185–201.

O'Neill, A., Matsuoka, T., Tsukada, K., 2004. Some pitfalls associated with dominant higher mode surface-wave inversion. Near Surface 2004 — 10th European Meeting of Environmental and Engineering Geophysics, Utrecht, The Netherlands.

Palmer, D., 2010. Are refraction attributes more useful than refraction tomography? Chapter book, "Advances in Near-Surface Seismology and Ground-Penetrating Radar.", SEG publications, in progress.

Park, C.B., Miller, R.D., Xia, J., 1999. Multichannel analysis of surface waves. Geophysics 64, 800–808.

Robertsson, J.O.A., Pugin, A., Holliger, K., Green, A.G., 1995. Effects of near-surface waveguides on shallow seismic data. 65th SEG, Meeting, Houston, USA, Expanded Abstracts, pp. 1329–1332.

Roth, M., Holliger, K., 1999. Inversion of source-generated noise in high-resolution seismic data. The Leading Edge 18, 1402–1406.

Scales, J.A., Smith, M.L., Treitel, S., 2001. Introductory Geophysical Inverse Theory. Samizdat press. available online (http://samizdat.mines.edu), 164 pp.

Van Veldhuizen, D.A., Lamont, G.B., 1998a. Multiobjective evolutionary algorithms: a history and analysis. Air Force Institute of Technology, Technical Report TR-98-03. 88 pp.

Van Veldhuizen, D.A., Lamont, G.B., 1998b. Evolutionary computation and convergence to a Pareto front. In: Koza, John R. (Ed.), Late Breaking Papers at the Genetic Programming 1998 Conference. Stanford University, pp. 221–228.

Van Veldhuizen, D.A., Lamont, G.B., 2000. Multiobjective evolutionary algorithms: analyzing the state-of-the-art. Evolutionary Computation 8, 125–147.

White, R.E., 1992. The accuracy of estimating Q from seismic data. Geophysics 57, 1508–1511.

Xia, J., Miller, R.D., Park, C.B., Tian, G., 2002. Determining Q of near-surface materials from Rayleigh waves. Journal of Applied Geophysics 51, 121–129.

Zhang, S.X., Chan, L.S., 2003. Possibile effects of misidentified mode number on Rayleigh wave inversion. Journal of Applied Geophysics 53, 17–29.